AIAA 98-0328

BOUNDARY LAYER FLOW CONTROL WITH A ONE ATMOSPHERE UNIFORM GLOW DISCHARGE SURFACE PLASMA

J. Reece Roth and Daniel M. Sherman
University of Tennessee, Knoxville, TN

and

Stephen P. Wilkinson
NASA Langley Research Center
Hampton, VA

36th Aerospace Sciences Meeting & Exhibit
January 12-15, 1998 / Reno, NV

AIAA 98-0328

BOUNDARY LAYER FLOW CONTROL WITH A ONE ATMOSPHERE UNIFORM GLOW DISCHARGE SURFACE PLASMA

J.Reece Roth* and Daniel M. Sherman†
University of Tennessee, Knoxville, TN 37996

and

Stephen P. Wilkinson‡
NASA Langley Research Center, Hampton, VA 23681

Abstract

Low speed wind tunnel data have been acquired for planar panels covered by a uniform, glow-discharge surface plasma in atmospheric pressure air known as the One Atmosphere Uniform Glow Discharge Plasma (OAUGDP). Streamwise and spanwise arrays of flush, plasma-generating surface electrodes have been studied in laminar, transitional, and fully turbulent boundary layer flow. Plasma between symmetric streamwise electrode strips caused large increases in panel drag, whereas asymmetric spanwise electrode configurations produced a significant thrust. Smoke wire flow visualization and mean velocity diagnostics show the primary cause of the phenomena to be a combination of mass transport and vortical structures induced by strong paraelectric electrohydrodynamic (EHD) body forces on the flow.

---

* Professor, Dept. of Electrical Engineering, Associate Fellow AIAA

† Graduate Research Assistant, Dept. of Physics and UTK Plasma Sciences Laboratory

‡ Aerospace Engineer, Fluid Modeling and Control Branch, Senior Member AIAA

Introduction

The use of magnetohydrodynamics (MHD) to control the turbulent viscous drag due to aerodynamic boundary layer flow has received considerable attention over the years. Most concepts have been based on ionized flow around a magnetized hypersonic vehicle, or on achieving such a plasma with ion seeding techniques. Numerous examples are found in patents awarded in the 1960's (see references 1 and 2). Emphasis has been placed on the magnetohydrodynamic approach in hydrodynamics due to the electrically conducting nature of seawater and perceived high economic or performance payoffs. However, in terms of a net energy balance, performance enhancement has proven elusive. An extensive review of pure MHD methods for drag reduction (i.e., those based exclusively on the cross product of the local current density and magnetic induction, **j** x **B**), through 1989 was compiled by Tsinober (ref. 3). Several current investigations are discussed in references 4 and 5 .

An alternative to MHD flow control which has received far less attention in the field of boundary layer research is based on the electric field alone, or electrohydrodynamic (EHD) control. In partially ionized gases the electric field itself, or the paraelectric effects associated

with an electric field gradient, can be used to accelerate ions and, via particle collisions (mobility drift), the neutral gas (references 6, 7). In the past, a difficulty with the EHD approach, especially in non-hypersonic flight applications, is generating an energy-efficient ionized flow near the surface. This report presents experimental data on the first aerodynamic application of a new EHD method based upon the One Atmosphere Uniform Glow Discharge Plasma or OAUGDP (refs. 6 to 13), that may change this situation.

The OAUGDP is a novel, surface-generated, atmospheric, RF (radio frequency) plasma. The concept of the device is discussed in detail later. The primary feature that distinguishes it from prior RF plasmas is its efficient ability to create a uniform glow discharge at atmospheric pressure on an extended flat surface. The electrodes required to do this have characteristics which lend themselves to practical engineering applications, such as simplicity and robustness. They should also be inexpensive and reliable. Given this capability, the goals of the present EHD study employing the OAUGDP for laminar or turbulent boundary layer control are twofold: 1) demonstrate the generation of EHD forces with magnitudes sufficient to alter boundary layer flow dynamics, and 2) demonstrate that such forces constitute a useful flow control mechanism.

Before introducing the OAUGDP and the current flow control study, however, some additional discussion of pure EHD controls will help to show why this approach has been chosen. An interesting feature of EHD controls, which perhaps is not generally appreciated, is that the electrostatic force on a charged particle can be significantly larger than the magnetic force on the same moving charge for practicable engineering values of magnetic and electric field strengths. This is an important point in view of potential aerospace flight applications. The maximum practical magnetic field from permanent magnets which can be expected in flush-mounted, non-obstructive surface application is estimated to be no more that about B = 0.1 Tesla. While higher values are obtainable with electromagnets, their Joulean dissipation (or superconducting refrigeration energy requirements) would seriously compromise any net energy saving in, for instance, a drag reduction application. The minimum electric field required to generate an OAUGD plasma in air is about E = 1.0 MV/meter (10 kV/cm). Assuming a typical commercial transport flight velocity of U = 300 m/sec, the force ratio on a singly charged particle is given by the quotient = E/UB = 3.3×10^4. In other words, the electric force on such a charged particle is more than four orders of magnitude greater than the maximum practicable magnetic force.

To examine the ratio of *body* forces, the magnitude of the electrical current and charged particle number densities must be considered as well. For the plasma considered in this report, a charged particle number density, $N_e = 1.0 \times 10^{17}/m^3$ is characteristic. A maximum current density corresponding to the glow-to-arc transition, $J = 10^4$ A/m^2, is assumed as a value not likely to be exceeded in any glow discharge plasma application. The body force ratio is then given by the quotient $r_B = qN_eE/JB$ where q is the electronic charge. This yields $r_B = 16$, or an EHD body force more than one order of magnitude greater than that of the MHD body force.

Another fundamental advantage of EHD forces is that the electric field can do work on the charged particles and, through strong collisional coupling at one

atmosphere, on the aerodynamic flow itself. A static magnetic field of force always operates orthogonally to the charged particle velocities, and therefore can do no work on the particles or the flow. For aerodynamic flow control applications, it is evident that EHD is the preferred approach. The obvious questions are how to effectively produce the requisite electrically charged medium at one atmosphere, and how to configure and drive the electric fields to produce effects that may be useful in such areas as drag reduction, heat transfer, lift, or flow separation.

An adequate number density of charged particles can be produced in an atmospheric glow discharge using a recently developed technology proprietary to the University of Tennessee Research Corporation. While under grant from the Air Force Office of Scientific Research, the first author was successful in producing the OAUGDP (Ref. 11), which is an extremely uniform, low frequency RF glow discharge that does not require either a vacuum environment or the mega- or gigahertz supply frequencies typical of industrial RF plasmas. The OAUGDP operates on the principle of the *charge-trapping* mechanism. Charge trapping refers to a specific, constrained, periodic oscillation of ions and/or electrons along electric field lines between a pair of flat electrodes which are characteristically side-by-side in flat panel aerodynamic applications. This electrostatic trapping may reduce plasma polarization, keep ions from knocking secondary electrons off the instantaneous cathode (which may initiate avalanches or breakdown), and prevent ions from heating the cathode surface and initiating a glow-to-arc transition.

Based on straightforward Lorentzian electrodynamic analysis of the plasma, the charge trapping mechanism identifies the pertinent independent variables, which include the electric field strength (E), electrode separation distance (d), type of gas, pressure (p), and RF electric field frequency (ν_o). A relation among these variables is given by Roth (section 12.5.2 in reference 6)

$$\nu_o \propto E/(pd) \qquad (1)$$

for the case of a parallel plate geometry. A planar strip geometry will have a similar but more complicated relation due to the arched field lines, but the same qualitative functional dependencies would be expected to prevail. The electric field E in Equation 1 may be approximated by the electrode potential, V, with E=V/d. Provided the operating parameters are in accordance with Equation 1, the OAUGDP will function at one atmosphere and produce a stable, steady-state glow discharge. A plasma thickness of one or two millimeters at power densities well below one watt per cubic centimeter was typical for the current experiments.

Equation 1 does not represent a finely tuned phenomenon and the parameters can vary over a useful range while maintaining the existence and uniformity of the plasma. If any of the parameters deviate significantly from Equation 1, however, either the OAUGDP will cease to function, or its uniformity will degrade into a filamentary discharge. The sensitivity of the OAUGDP to variations in the independent input parameters is a current subject of investigation at the University of Tennessee's Plasma Sciences Laboratory.

The magnitudes of the parameters in Equation 1 for bench top demonstration of the OAUGDP are easily attainable. For instance, a frequency of several kilohertz, an rms voltage of several kilovolts, and a planar strip separation

distance of 5 or 10 mm are adequate to initiate the plasma at atmospheric pressure. The OAUGDP is not hard-starting, and does not require external initiation with a Tesla coil or spark gap. While the dissipative (or plasma) current in the OAUGDP is small (about 0.030 amp rms in these experiments), without special impedance matching the reactive, non-dissipative current can be large (approximately 0.4 amp rms) and the power source must be sized accordingly.

The absence of any large dissipative currents due to filamentary breakdown or arcing in the OAUGDP plasma allows it to operate at low power levels, consistent with the possibility of net energy savings in flight boundary layer flow control or drag reduction applications. For example, a characteristic boundary layer viscous dissipation value for a long range commercial transport has been estimated to be roughly 5000 watts per square meter (737-class airplane at cruise conditions). By comparison, in bench top tests, the OAUGDP can operate with a power of 320 W/m^2 or less based on the measured, non-reactive power and the surface area covered by the plasma. While there is no evidence or claim at this time that such a low power level can effectively control, say, a turbulent boundary flow at high Reynolds number flight conditions, the energy cost of sustaining a uniform layer of glow discharge plasma over a large area is nonetheless very low.

This low energy cost occurs for a fundamental reason: the OAUGDP has been shown to be a glow discharge, created twice during each RF cycle (see refs. 12, 13). As a glow discharge, the ionization process in the instantaneous cathode region occurs at the Stoletow point, which is about 81 electron-volts(eV) per ion-electron pair for air (Ref. 6, Section 8.3.4). This is, in principle, the lowest possible energy cost of producing an ion-electron pair in a plasma source, and compares very favorably with the energy cost of other atmospheric plasma sources, such as plasma torches or arcjets, for which the energy cost is about 10,000 eV/ion-electron pair.

Regarding applications, the OAUGDP is quenched by liquid water, although it recovers rapidly from a water spray. The usual ranges of atmospheric, climatic humidity conditions are acceptable although high, near condensing levels have not been investigated. Only dry, high altitude applications are currently envisioned.

The OAUGDP is fundamentally different from ion wind concepts that rely on a corona discharge as an ion source. Malik, et al. (ref. 14) used the ion wind technique in a flat plate DC "brush" discharge fashion and were able to secure a small reduction in measured drag of about 5% for a turbulent boundary layer flow at a length Reynolds number of approximately one million. Research was later abandoned, however, due to inability to scale the operation of the hardware to flight conditions. More recently, El-Khabiry and Colver (ref. 15) were able to produce up to 50% or more viscous drag reduction in very low Reynolds number flows (on the order of 10^5) using a corona discharge between spanwise wires on a flat surface for both DC and low frequency (60 Hz) AC excitation. Each of these techniques is probably limited to low Reynolds number applications due to limitations on scaling the corona discharge effect to higher flow velocities. The OAUGDP, however, is more readily scaleable and has the potential to function at much higher Reynolds numbers.

With an efficient source of surface plasma, the challenge becomes how to

effect a useful EHD flow control mechanism in a boundary layer, particularly a turbulent boundary layer. Initial investigations were aimed at understanding the basic response of a boundary layer to several simple, planar electrode configurations that can be used to produce the OAUGD plasma. These consist of streamwise and spanwise arrays of flush-mounted strip electrodes on a flat panel, all at the same RF potential and phase with respect to a ground plane or electrode on the opposite side of the panel.

Experimental Apparatus

Low speed wind tunnel tests of panels with the OAUGD plasma were conducted in the NASA Langley 7x11 Inch Low Speed Wind Tunnel (7x11) to determine the basic response of boundary layer flow to the plasma for a few simple panel configurations. The 7x11 is a closed return, unpressurized air facility with a test section 178H x 279W x 914L millimeters. A 305 x 279 millimeter central portion of the lower test section wall was used for testing. Tests included the directly measured viscous drag of flat plate panels with the OAUGD plasma generated on the surface, vertical (wall-normal) boundary layer pitot pressure profiles measured a short distance downstream of the panels, and smoke flow visualization tests. The air-bearing drag balance used and a general view of the tunnel test section is shown in Figures 1a and 1b. The semi-catenaries shown in Figure 1a are high voltage power leads to the plasma panels. They consist of brass-ball utility chains (commonly used for light switch pull chains, etc.) and were chosen for their extreme flexibility, electrical conductivity, and lack of any sharp, corona-producing features. By exerting equal and opposite horizontal forces on the drag balance, the forces due to the power leads approximately cancel out. Any small remaining residual force is well within the linear range of the instrument and is accounted for in the no-flow drag tare readings.

The smoke wire was 0.1 mm diameter type 304 stainless steel and was stretched across the width of the test section at a variable height above the wall. A weight and pulley arrangement kept the wire taut during heating. It was powered by a variable DC power supply with a 100 vdc maximum output (typical range at 4 m/s was 40-50 vdc). The "smoke" was the vapor of common mineral oil. Smoke wire photographs were obtained by firing an electronic flash during the vertical blanking period of a full frame, monochromatic digital video camera (8-bit resolution, 768 by 484 pixels), at a variable delay time after energizing the smoke wire. The delay time was determined by trial and error. Video pixel data were downloaded from the digital camera to a computer for processing.

For velocity profiles, a slender, tapered total pressure pitot tube was traversed across the boundary layer height downstream of the energized plasma panels. The tip was fabricated from flattened, stainless steel hypodermic tubing. The tip height was 0.28 mm and the width was 0.65 mm. The probe was far enough downstream of the energized panel to prevent any electrical arcing to the instrument. The initial height of the probe above the wall was set by monitoring electrical contact between the probe and metallic wall. The probe was raised through the boundary layer with an automated stepping motor-driven slide mechanism in 0.5 mm increments. A typical profile was acquired quickly (in about 30 seconds) to prevent heating the panels, which could cause their adhesive backing to weaken and release. Pitot differential pressure was measured

between the probe and a static pressure port of the tunnel wall with a high accuracy capacitive or piezoelectric gauge.

Figure 2 shows a plan view sketch of a typical panel. The panels were constructed from conventional dielectric printed circuit board material (woven-glass/epoxy construction, 0.75 mm thick, double-sided, 1 ounce copper coating). The plasma-generating electric field lines arch over the upper surface of the board (where the plasma is generated) and traverse the board thickness. In the more recent designs, an array of electrode strips was etched on the top (flow) side of the board and the bottom surface left as a uniform copper plane as illustrated in Figure 2. Alternately, an asymmetric array of electrode strips was etched on the bottom of the panel when it was desired to accelerate or decelerate the boundary layer flow. The geometrical configurations of the various panels used in this study are shown in Figures 3a through 3c.

For all tests, the flow passed over the copper electrodes with no additional dielectric coating. Since the OAUGDP charge trapping mechanism operates on displacement rather than real electrical currents, this surface can, if desired, be covered with a thin insulating and/or protective layer without qualitatively affecting the results reported herein. The circuit board was attached to a 12.7 mm thick fiberglass backing board (type G-10) with double-sided adhesive tape to make the panel structurally rigid but still capable of being disassembled. The designation code and electrode dimensions of the various panels reported on in this paper are listed in Table 1.

The parallel electrode strips on the top of the panel were bussed together and connected to one power supply terminal and the lower plane or electrodes underneath the panel to the other terminal. The parallel electrode strips on top of the panel were generally at high voltage, while the lower electrode was grounded, although configurations with the opposite polarity would also produce plasma and the effects reported below. A high voltage (up to 5.4 kV), low frequency RF (up to 20 kHz) power supply was used with its transformer output connected directly to the panel without a special impedance matching network.

Figure 4 is a plan view photograph of a panel energized (plasma activated but with no flow) and is representative of the technique. The 0.5 mm solid, horizontal, dark strips are the parallel copper electrodes. The gray-scale regions to either side of the electrodes are the OAUGD plasma. The plasma was visually extremely uniform.

For the drag tests, the panel was mounted on an air bearing drag balance located below the tunnel test section, with the panel forming the central section of the lower wall. The boundary layer flow was tripped near the outlet of the tunnel's contraction with a 1.07 mm circular rod on the test wall 575 mm upstream of the leading edge of the panel. Small (0.25 mm) gaps around the test panels allowed them to float freely on the drag balance. A pressure control box around the test section allowed the static pressure in the test section to be matched to the control box pressure. This minimized errors in drag measurements by reducing flow in the gaps surrounding the panels.

Procedures and Results

Data for streamwise and spanwise electrode orientations were acquired, as well as paired comparison drag data for both the plasma-energized and unenergized (approximate smooth flat plate drag) conditions. Data were also

taken on panels with asymmetric arrays of electrodes such as those shown in Figure 3b to study the acceleration and deceleration of the flow in the boundary layer, and the consequent drag decrease or increase (respectively) compared to the unenergized flat plate. Data on drag increase or decrease were measured as parametric functions of the flow velocity (up to 26 m/s), electrode voltage (up to 5.4 kV rms), and RF frequency (from 500 to 8000 Hz).

The direction and magnitude of the paraelectric plasma-induced acceleration of the flow is determined by the direction of the electric field gradients, and these are in turn strongly influenced by the orientation and details of the electrode geometry. The preliminary data reported here are for unoptimized electrode geometries. It is anticipated that with additional modeling studies, geometrical optimization will increase the magnitude of the effects reported at a given set of plasma operating parameters. In addition, the electrodes in this study were energized with a single phase of RF excitation. This produces EHD body forces which are the result of averaging attractive and repulsive forces over the RF cycle, a *second order* effect. Much stronger effects should be possible when adjacent electrodes are excited with polyphase RF power, providing a DC electric field parallel to the surface, a *first order* EHD effect.

In this paper, data are presented for three principal cases: *laminar data,* for which the wind tunnel flow was laminar before encountering the panel; *transitional data* corresponding to about 75% intermittency at the upstream edge of the model, and fully *turbulent data.* Since the boundary layer flow was tripped upstream of the panel, there was actually no case of completely undisturbed laminar flow. At low tunnel velocities, however, the flow was laminar (but with occasional unsteady oscillations) as evidenced by smoke wire pathline visualization and the absence of any turbulent breakdown in diagnostic hot wire signals.

Representative results from a panel with symmetric electrodes, each electrode a copper strip 0.5 mm wide with centers spaced 10.5 mm apart, are shown in Figure 5a for the streamwise electrode orientation (panel C7-A), and in Figure 5b for the spanwise electrode orientation (panel C7-C). Each of these displays the expected power-law Reynolds number dependence for the "plasma off" condition. Note the change in slope of the "plasma off" curve in Figure 5a or 5b in the range of 7-8m/s, corresponding to transition from laminar to turbulent flow. For the "plasma on", streamwise electrode case, a substantial increase in drag is observed. This is due to several factors. As will be shown, the plasma excitation for velocities below about 7 m/s (laminar region) trips the flow to full turbulence, partially explaining the drag increase in that region. The drag increase persists, however, to the highest attainable velocity of the wind tunnel indicating that more than just flow tripping is involved. For the "plasma on", spanwise electrode case, a smaller drag increase is produced and only in the laminar/transitional region. The difference in behavior between the two cases along with evidence presented later in the paper suggests the formation of strong, EHD-driven, streamwise vortical structures in the boundary layer for the streamwise-oriented electrode case.

The very small differences in surface configuration among different panels did not measurably affect (beyond the intrinsic precision of the data) the drag for the unenergized panels reported in this paper. Despite the small roughness introduced by the copper electrodes on the panel surfaces, relative to the energized

cases, the unenergized models behaved as smooth flat plates.

It was observed that when the panels with electrode orientations parallel to the flow were energized, the presence of the OAUGDP was a strong promoter of full boundary layer turbulence. If the flow was laminar at the panel leading edge, energizing the plasma for either the spanwise or streamwise electrode case would trip the flow. This is illustrated in Figures 6a and 6b, smoke wire visualizations at a height of 5 mm of the flow over panel C7-A (the streamwise electrode counterpart of panel C7-C shown in Figures 2 and 4). Figure 6a shows the smoke wire pathlines for a stream velocity of 4 m/s at a height of 5 mm above the surface. The panel is energized at 3.0 kHz and 3 kV rms. The convergence of the smoke pathlines toward the electrodes, the apparent subsequent formation of vortical structures, and the breakdown into turbulence are all clearly evident. Figure 6b shows the same conditions as Figure 6a, but at a higher electrode voltage of 5 kV rms. Because of the higher electric field at this voltage, the vortical structures develop sooner, are more compact, and break down sooner. The presence of the plasma generated by the symmetric electrode configuration constitutes a very strong tripping mechanism.

Figure 6c shows the smoke pathlines for the case of a single, isolated streamwise electrode above a planar lower electrode. The electrode strip is 0.5 mm wide. The velocity is 4 m/s and the wire height in this case is 2 mm. Near the leading tip of the electrode, the smoke pathlines appear initially to symmetrically converge towards the electrode, forming counter-rotating vortical structures which quickly become turbulent. This process occurs along the length of the electrode, giving rise to the spreading effect observed. Figure 6c is further evidence of strong EHD forces in play. (Also observed in Figure 6c are quasi-two-dimensional wave crests upstream and to the sides of the vortical structures. These waves were also present without the plasma, and are presumed to be laminar instability waves (TS waves) associated with other flow disturbances, i.e. the disturbances input by the boundary layer trip upstream of the test section or even the smoke wire itself. They have no significant relation to the EHD forcing or streamwise vortical structure formation.)

For each of the early plasma panels, it was observed that a small electrostatic drag (by comparison with the viscous drag usually measured) was observed, which is unrelated to the flow. This drag is induced by electric field lines terminating on the panels with or without a plasma present, and is present even in the absence of a flow. This electrostatic drag arises from the electrodynamic stress tensor, in which the electric field lines can be visualized as acting in tension between the panel electrodes and the grounded surroundings, producing an electrostatic pressure and an rms average force on the panel. The measured drag must (and was) corrected for this electrostatic, non-flow-related drag. The electrostatic drag (or electrostatic pressure) follows a quadratic relationship between the applied rms excitation voltage and measured drag. Figure 7 is a representative plot of the electrostatic drag force for panel C1-B. By replacing metallic with non-metallic surfaces near the panel and drag balance, the magnitude of the electrostatic drag shown in Figure 7 was reduced to insignificant levels in the more recent data. All drag data presented in this paper were corrected for electrostatic drag when it was above the resolution of our drag measurements (about 10 milligrams).

Vertical boundary layer velocity profiles were also measured with a total pressure probe on several panels with symmetric as well as asymmetric electrode configurations. Figure 8 presents velocity profiles for Panel C7-A (with symmetric, streamwise electrodes) one-half way between two adjacent electrodes, for the case of laminar (a), transitional (b) and fully turbulent (c) flow at the panel leading edge. The probe tip was located approximately one boundary layer thickness downstream of the model over the smooth aft filler plate of the lower wall. (A metallic aft plate was used for the profile measurements to aid probe initial height determination; for drag measurements, a non-metallic plate was used to minimize electrostatic drag error.) Figure 9 presents similar data, also from the streamwise electrode configuration, with the pitot probe directly behind one of the streamwise electrodes. Figure 10 shows the profiles downstream of spanwise oriented electrodes on panel C7-C.

The profiles for the streamwise case (Figures 8 and 9) show a dramatic alteration of the flow due to interaction with the plasma that diminishes with increasing velocity. There is a large acceleration of the flow near the wall and a retardation farther out. The cases of the probe between and behind the electrodes are qualitatively similar, but differ in magnitude. Smoke wire (e.g., Figures 6(a,b)) and hot wire diagnostics show that the energized, streamwise electrode patterns effectively trip the flow, and that any between-electrode/behind-electrode differences are largely mixed out at the end of the panel. For the spanwise case in Figure 10, the effect is largely limited to the laminar flow condition, with little effect in the transitional case and virtually no discernible effect in the turbulent case. (The step-wise appearance of the data in Figure 10(a) is an error due to a mismatch between the pressure sensor and A/D converter ranges. The trend of the data is valid.)

The profiles corroborate the drag and smoke wire data. For the streamwise electrode case, there is a substantial retardation of the profile affecting the entire boundary layer. This increases the boundary layer momentum deficit and qualitatively corresponds to the large increase observed in the drag in Figure 5a. For the spanwise electrode configuration shown in Figure 10, a significant effect is evident only in the laminar regime, with a similar effect on the drag (Figure 5b). For the smoke wire flow visualization, the eruption of vortical structures observed in Figures 6a and 6b appears to be consistent with the flow retardation observed in the velocity profiles of Figures 8 and 9.

Figure 11 shows the instantaneous RF voltage and current for panel C1-C operated at an rms voltage of 1.4 kilovolts, and a frequency of 2.5 kilohertz. The voltage was measured at the power supply output with a high voltage probe having the requisite frequency response. The current through the high voltage power cable was measured with a high bandwidth, toroidal current transformer with a sensitivity of 1 volt/amp. The noisy region at the positive peaks of the current waveform represents the plasma initiation, during which a classical, "DC", normal glow discharge briefly exists between the electrodes (Refs. 12, 13). The plasma ignition appears only once per cycle for the model and conditions portrayed in Figure 11. For most models studied during these tests, however, plasma ignition occurred twice per cycle (see Introduction). There was a noticeable variability in the current waveforms for the various panels and excitation voltages, which are the subject of ongoing study.

A final observation applicable to all of the current OAUGDP flat panels relates to acoustics. Each panel exhibited a strong audible tone at the RF excitation frequency. The tone was present in unconfined bench-top testing of the panels as well as in the enclosed wind tunnel test section, ruling out any resonant chamber effects. It was initially suspected that the OAUGDP might be exciting a panel resonance. However, monolithic mounting of the panel to its baseplate did not appreciably change the pitch or intensity of the tone. The emitted sound therefore must be considered a direct coupling of the OAUGD plasma formation mechanism into radiated acoustic energy, a further indication of strong plasma-neutral gas coupling.

Drag Reduction Data

Probably the most interesting data taken during this study were those from the asymmetric panels which were designed to unidirectionally accelerate the flow. The smoke flow visualization of Figures 6a and 6b with symmetric electrodes indicate an attraction of the flow toward the electrodes. If the electrodes are fabricated in an asymmetric manner, such as the geometry illustrated in Figure 3b, an unbalanced paraelectric EHD body force is exerted on the plasma/flow field, and a corresponding force is exerted on the panel on which the electrodes are mounted. (The term *paraelectric* refers to the fact that the observed attraction of the smoke towards the electrode is independent of the instantaneous electric polarity of the electrode. It is used in the same sense as the more familiar phenomenon of *paramagnetism*). The resultant force can be in the direction of the airflow (co-flow), or opposite the free stream flow (counter-flow) depending on the orientation of the electrode asymmetry.

Figure 12 illustrates the production of a force (thrust in this case) by panel E6-C mounted on the wind tunnel drag balance, but with no flow. Due to previously mentioned wind tunnel modifications, the electrostatic drag correction is insignificant. The plasma was operated at 3.0 kilohertz and the electrode spacing was 8.5 mm between the centers of spanwise electrode strips each 0.5 mm wide. The asymmetric strips on the bottom of the panel were located at only one side of the top electrode strips. These bottom strips were 3.0 mm wide, and separated streamwise from the top strip by about 0.25 mm. This is not necessarily (and is probably not) an optimum geometrical configuration to produce thrust, but nonetheless illustrates the asymmetrical force effect.

Figure 13 presents the drag on panel E6-C (the same model used in Figure 12) over the usual laminar, transitional and turbulent velocity ranges. The plasma was operated at 3.0 kilohertz and 4.0 kilovolts rms. The two curves corresponding to the unenergized cases are virtually coincident, and represent the smooth flat plate reference drag data. The lower curve shows an (unoptimized) reduction in drag comparable to the plasma generated thrust. The upper curve was taken with the same panel rotated 180 degrees to generate a plasma-induced drag on the plate.

Figure 14 shows the difference between the plasma-on and plasma-off drag for the asymmetric panel E6-C in both the co-flow and counter-flow velocity fields. Note that the ordinate of Figure 14 is the absolute value of the drag difference. For the counter-flow case, the 0.9 +/-0.05 gram drag increase is approximately constant across the speed range of the tunnel. This indicates that the plasma-induced, counter-flow EHD force is additive and the effect is primarily

propulsive. For the case of the co-flow orientation, however, a trend exists below 10 m/s indicating a clear Reynolds number dependence. The plasma has been noted in all cases to trip the boundary layer so the Reynolds number dependency shown in Figure 14 could be more boundary layer trip related than turbulence modification related. Nonetheless, this finding along with other data presented in this report point to the possibility of using the newly discovered EHD forcing to target and control boundary layer turbulence.

Model E6-C was not optimized for the EHD force. While the predominant plasma forms on the upper surface over the lower surface electrode, flow visualization has shown that a small amount of plasma forms on the opposite edge of the upper surface electrode due to field lines wrapping around to the lower electrode. The net effect is to have a large EHD force in one direction (downstream in the co-flow case) and a smaller force in the opposite direction.

The asymmetric panel E6-C was mounted in the wind tunnel without flow, but with the pitot tube positioned at the same location used in Figures 8-10. The resulting blowing velocity profiles are shown in Figure 15 for electrode voltages of 3, 4, and 5 KV rms. Maximum plasma-induced velocities up to 4.0 meters/sec were observed. Particularly interesting were the induced velocities of up to 0.5 meters/sec at distances at least 3 cm from the wall, which occurred for all driving voltages.

Figure 16a and 16b are photographs of the influence of the OAUGDP on a laminar jet of smoke injected above a single, asymmetric electrode arrangement. The test was conducted in a still air chamber. The "smoke" in this case was actually titanium tetrachloride (a commonly used white flow marker chemical) injected manually in a slow,. steady stream from a plastic squeeze bottle. The plasma is not visible in Figure 16 due to the strong illumination required for the smoke. The paraelectric forcing in Figure 16b causing the jet to deflect towards the electrode is evident.

In terms of a phenomenology, the flow of the smoke and the air which it marks responds to paraelectric EHD effects in the following way. In Figure 16b, the flow is drawn downward by a low pressure above the low electric field gradient region of the plasma, entrained in the ion-driven plasma flow toward the region of high electric field gradient, and forced outward by the region of high (plasma stagnation) pressure along the surface of the panel. The flow is rapidly accelerated away from the region of high gas pressure and high electric field gradient (primarily to the left of the electrode due to the asymmetry but also to a lesser degree to the right as well). This effect is responsible for the blowing velocity profiles illustrated in Figure 15.

The behavior shown in Figure 16b is consistent with a pure paraelectric effect on the plasma and on the flow which it entrains. It is not a classical case of dielectrophoresis, although similarities exist. Dielectrophoresis refers to the forces on neutral, polarizable, dielectric material when subjected to a spatially non-uniform or a time-varying electric field (ref 16). In the current case, no smoke or air movement is observed until sufficient voltage is reached for the plasma to initiate. This indicates a different phenomenon than dielectrophoretic behavior alone. It is clear that the underlying mechanism for neutral gas movement in the presence of the OAUGD plasma warrants further theoretical and experimental study.

Accuracy of Experimental Data

The primary experimental data measured during this investigation were pressure (for velocity) and force (for drag). Pressures were measured with capacitive or piezoelectric transducers with better than 0.1% accuracy and read on 5 1/2 digit digital voltmeters with an order of magnitude or better accuracy than the pressure transducers. Given additional sources of error such as the data reduction model, probe alignment and position, probe viscous effects, and electronic voltage offsets and noise, the overall accuracy is still estimated to be within no more than +/-2% of the actual value, which was adequate for the current tests. The force on the drag balance was measured with an elastic piezoresistive force sensor with two active resistor elements. Two passive resistors were added to complete a bridge circuit. The bridge offset was amplified, filtered with a 4th-order Butterworth low pass filter at 0.5 Hz, and calibrated against an applied streamwise force. The resultant resolution was about 10 milligrams. The absolute, systematic error is estimated to be less than 5% of the actual value and much better for comparative measurements.

Discussion

The goals of this study, as discussed in the introduction, were to demonstrate that EHD forces could be generated of sufficient magnitude to alter wall turbulence and drag, and to demonstrate that such forces can lead to a useful control mechanism. The first goal was clearly met, and was limited only by the voltage of the power supply. The latter must also be considered a success, since it has been demonstrated that EHD forcing can generate significant body forces on the neutral gas flow. The usefulness of the flow forcing demonstrated thus far will of course depend upon application-specific studies. Also, the likelihood that the observed paraelectric behavior is a second-order effect compared to polyphase electrode excitation holds further hope for useful engineering applications (see Ref. 10).

Several key questions were addressed by the diagnostics conducted during this study. The cause of the dramatic drag increase which occurs for the symmetric streamwise electrode arrays (Figure 5a) is clearly associated with formation of the symmetric streamwise vortical structures evidenced by both the smoke wire flow visualization (Figure 7) and the pitot tube velocity profiles (Figures 8 and 9). Conversely, the much smaller drag increase associated with the symmetric, spanwise arrays (Figure 5b) results from the lack of streamwise vortex formation and advance tripping of the turbulent boundary layer on the panel. For the case of the asymmetric spanwise electrode panels (e.g., model E6-C), the directed thrust leading to a drag increase or decrease results from the same mechanism that causes the vortex formation in the streamwise, symmetric case. This is clear from the still air smoke flow visualization (Figure 16) and the no-flow blowing profiles (Figure 15).

The possibility of a local wall heating mechanism deserves closer attention, but is not a primary mechanism responsible for the observed model behavior. The OAUGDP is not a high energy density plasma, and does not generate a great deal of heat. Power input levels to the plasma were no more than about 100 mW/cm^2, based on the electrode array area. After several minutes of operation the panels become sensibly warm to the touch but certainly not enough to explain any of the dramatic changes in drag, velocity profiles, or smoke flow patterns. A cursory measurement of boundary

layer temperature downstream of an energized model showed only a small temperature rise of several degrees Celsius. A more pertinent question would be the magnitude of the localized electron temperature within the plasma and its impact on the observed phenomena. However, this is beyond the scope of current investigations.

Figures 8 and 9 show that the effect on the plasma is spread across the entire boundary layer for the streamwise symmetric electrode case. It seems clear that a major vortex-dominated mechanism is in play. This is evidenced by direct manipulation of the streamwise flow by EHD forces in the (initially) laminar smoke wire data shown in Figure 6.

Future Plans

A strong paraelectric EHD effect on boundary layer flow has been demonstrated, and opens the way to refinements and new configurations which may lead to useful applications. Immediate plans are to extend the current work to more specific active control investigations based on either accelerating the flow in a steady fashion, or oscillating the flow in the spanwise direction. The later technique is suggested by recent studies (e.g., ref. 17) showing that oscillating a turbulent boundary layer in the spanwise direction can have a dramatic effect on reducing turbulence intensity and drag. While control of wall turbulence and drag was the subject of the current investigations, other possibilities in areas such as heat transfer, lift enhancement, and flow separation control are also of interest.

Finally, in terms of Bushnell's "Designer Fluid Mechanics" (Ref. 18), the EHD approach has successfully negotiated his technical/scientific filter by demonstrating the ability to move a neutral gas with EHD forcing to reduce or enhance drag, or significantly alter the velocity profile of the boundary layer. Beyond this, future efforts need to be directed at passing through Bushnell's second filter, that of technological feasibility. This entails demonstrating such factors (where not already demonstrated) as simplicity, economy, retrofittability, mechanical passivity, and robustness and reliability. It also means demonstrating the ability to simulate the processes and mechanisms in such a way as to make possible developmental work on small inexpensive models in ground facilities. In addition, much future work needs to be done to characterize, parameterize, and understand the physical processes both in the OAUGDP and with respect to the paraelectric EHD effects responsible for the plasma-flow interaction.

Summary

The first aerodynamic data from planar panels with a uniform glow discharge surface plasma at atmospheric pressure (known as the One Atmosphere Uniform Glow Discharge Plasma or OAUGDP) have been acquired. Flat plate panels with either streamwise or spanwise arrays of flush, closely spaced symmetric or asymmetric plasma-generating surface electrodes were studied with laminar, transitional, and fully turbulent boundary layer flow in a low speed wind tunnel. It was observed that EHD forces can produce dramatic effects, arising from paraelectric, RF forcing of the flow. Notable effects include large increases in measured drag due to either vortex formation (symmetric electrode case) or directed thrust (asymmetric electrode case). In the more dramatic cases, the entire thickness of the boundary layer was affected by either flow acceleration or retardation. The effects of heating are discounted and the primary cause of the

observed flow phenomena attributed to electrohydrodynamic (EHD) forcing of the flow by a paraelectric RF body force.

Acknowledgments

This research was a collaborative study by the University of Tennessee, Knoxville and NASA Langley conducted under the auspices of the Chief Scientist (D. M. Bushnell), NASA Langley Research Center, Director's Discretionary Fund. The work of the first and second author was supported under NASA Langley Cooperative Agreement NCC-1-223.

References

1. Clauser M. U. and Meyer R. X.: "Magnetohydrodynamic Control Systems", US Patent 3,162,398, Issued Dec. 22, 1964.

2. Hill, G. A.: "Ionized Boundary Layer Fluid Pumping System", US Patent 3,095,163, Issued June 25, 1963.

3. Tsinober, A.: , "MHD Flow Drag Reduction", in Viscous Drag Reduction in Boundary Layers, AIAA Progress in Astronautics and Aeronautics, Vol. 123, Seabass A. R., ed., ISBN 0-930403-66-5, pp. 327-349.

4. Nosenchuck D.M., Brown G.L., Culver H.C., Eng, T.I. and Huang I.S.: "Spatial and Temporal Characteristics of Boundary Layers Controlled with the Lorentz Force," Proceedings of the Twelfth Australasian Fluid Mechanics Conference, Vol. 1, pp. 93-96, Sydney, NSW, Australia, December 10-15, 1995.

5. Kral, L. D. and Donovan J. F.: "Numerical Simulation of Turbulence Control Using Electromagnetic Forces," Proceedings of the 1996 ASME Fluids Engineering Conf., Forum on Control of Transitional and Turbulent Flows, July 7-11, 1996.

6. Roth, J. R.: Industrial Plasma Engineering, Volume 1 - Principles. Institute of Physics Publishing, Bristol and Philadelphia, ISBN 0-7503-0318-2 , 1995 , pp. 453-461.

7. Roth, J. R.; Liu, C.; and Laroussi, M.: "Experimental Generation of a Steady-State Glow Discharge at Atmospheric Pressure," Paper 5P21, 19th IEEE International Conference on Plasma Science, Tampa, FL, June 1-3, 1992.

8. Roth, J. R.; Tsai, P. P.; and Liu, C.: "Steady—State, Glow Discharge Plasma," U. S Patent # 5,387,842, Issued February 7, 1995.

9. Roth, J. R.; Tsai, P. P.; Liu, C.; Laroussi, M.; and Spence, P. D.: "One Atmosphere, Uniform Glow Discharge Plasma." U. S Patent 5,414,324, Issued May 9, 1995.

10. Roth, J. R. (1997): "Method and Apparatus for Covering Bodies with a Uniform Glow Discharge Plasma and Applications Thereof". U. S. Patent #5,669,583, Issued September 23, 1997.

11. Roth, J. R.: "Investigation of Uniform Glow Discharge in Atmospheric Air," AFOSR Final Scientific Report, PSL-95-4, April 1, 1994-March 31, 1995.

12. Ben Gadri, Rami: "Numerical Simulation of an Atmospheric Pressure and Dielectric Barrier Controlled Glow Discharge", Doctorat (Ph.D.) of the University Paul Sabatier of Toulouse, France. Order Number : 2644, 30 April, 1997.

13. Massines, F.;Ben Gadri, R.;Rabehi, A.; Decomps, Ph.; Segur, P.; and Mayoux, Ch.: "Mechanisms of a Glow Discharge at Atmospheric Pressure Controlled by Dielectric Barrier", Journal of Applied Physics. (accepted and in press, 1997).

14 . Malik, M. R., Weinstein, L.M., and Hussani, M. Y., "Ion Wind Drag Reduction", AIAA Paper 83-0231, 1983.

15 . El-Khabiry, S. and Colver, G. M.: "Drag Reduction by DC Corona Discharge Along an Electrically Conductive Flat Plate for Small Reynolds Number Flow". Phys. Fluids, Vol. 9, No. 3 (1997) pp 587-599.

16. Pohl, H. A.: "Dielectrophoresis, The Behavior of Neutral Matter in Nonuniform Electric Fields", Cambridge University Press, 1978, ISBN 0-521-21657-5, pp. 6-18.

17. Jung, W., Mangiavacchi, N. and Akhavan, R.: "Suppression of Turbulence in Wall-Bounded Flows by High Frequency Spanwise Oscillations", Phys. Fluids A. vol. 4(8), pp 1605-1607, 1992.

18. Bushnell, D. M.: "Application Frontiers of 'Designer Fluid Mechanics' - Visions versus Reality or an Attempt to Answer the Perennial Question 'Why isn't it Used?'", AIAA Paper 97-2110, 28th AIAA Fluid Dynamics Conference, June 29-July 2, 1997, Snowmass Village, CO.

Table 1. Panel Designations and Electrode Dimensions

Panel#	Orientation	Arrangement	Electrode Width	Electrode Pitch*
C7-C	Spanwise	Symmetric/planar	0.5 mm	10.5 mm
C7-A	Streamwise	Symmetric/planar	0.5	10.5
C1-B	Streamwise	Symmetric/staggered	2.0	8
E6-C	Spanwise	Asymmetric/staggered	0.5	8.5

* center-to-center spacing of electrodes

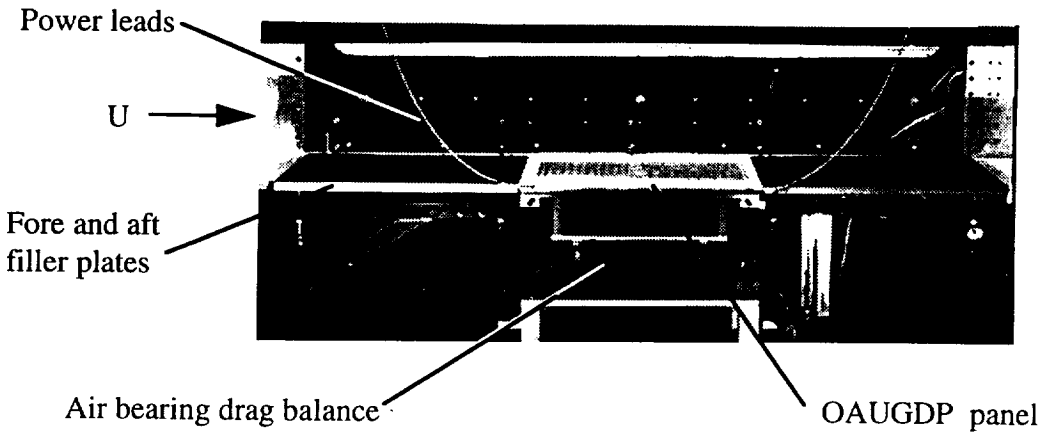

Figure 1a. NASA Langley 7x11 Inch Low Speed Wind Tunnel. Plasma panel (unenergized) on drag balance in wind tunnel test section (front and top walls of test section removed for clarity)

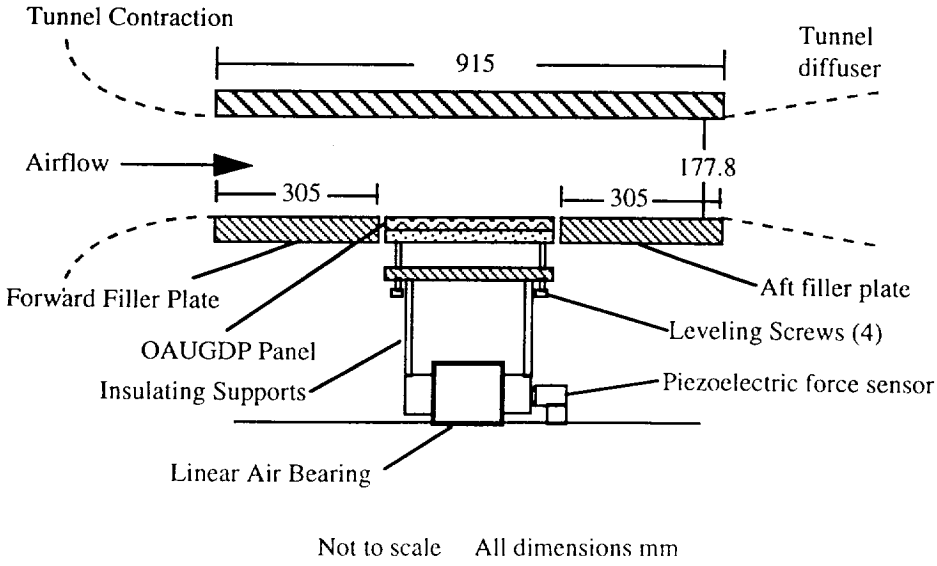

Figure 1b. Streamwise cross-sectional sketch of 7x11 Inch Low Speed Wind Tunnel test section.

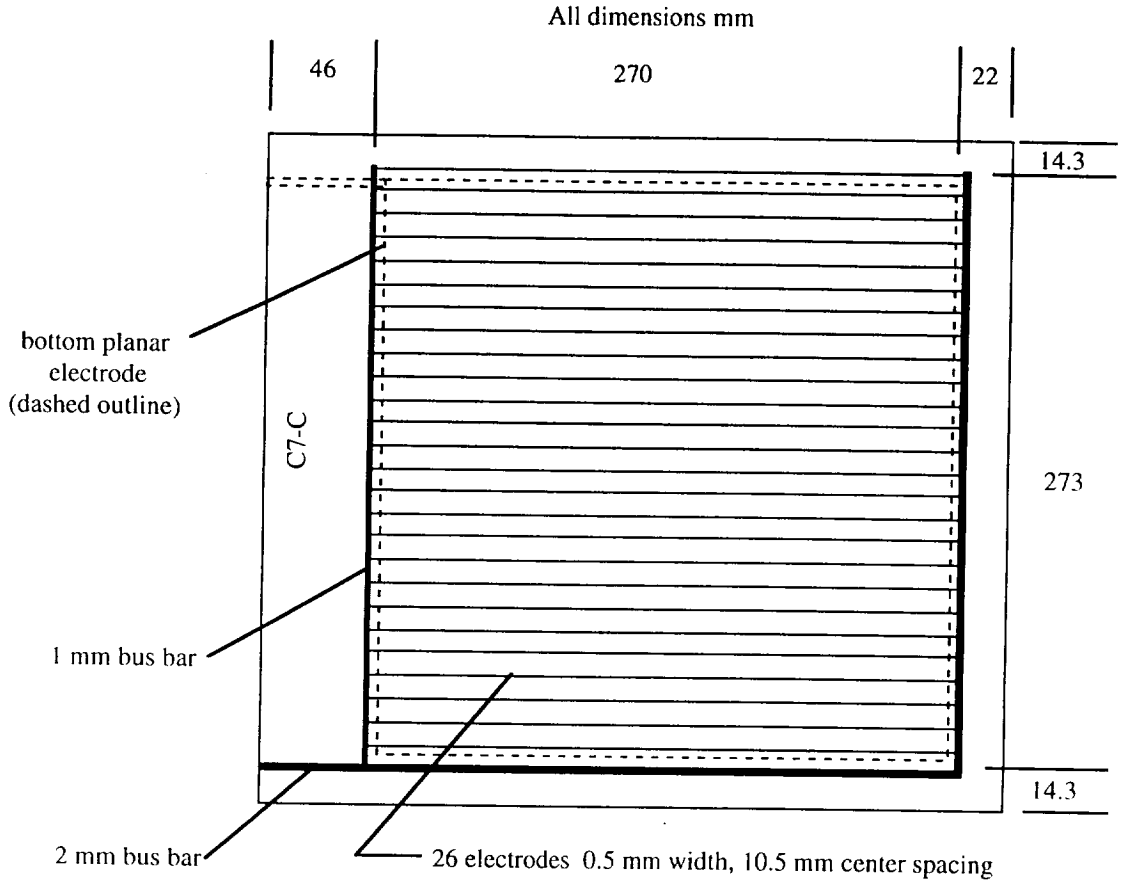

Figure 2. Dimensioned sketch of panel C7-C

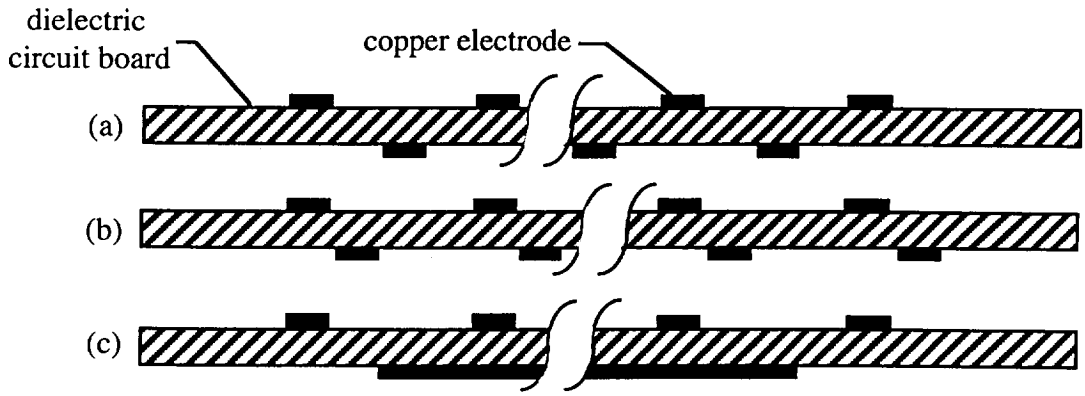

Figure 3 (a-c). Cross-sectional sketch of plasma panel concepts. (a) symmetric, staggered lower electrodes, (b) asymmetric, staggered lower electrodes, (c) symmetric, planar lower electrode

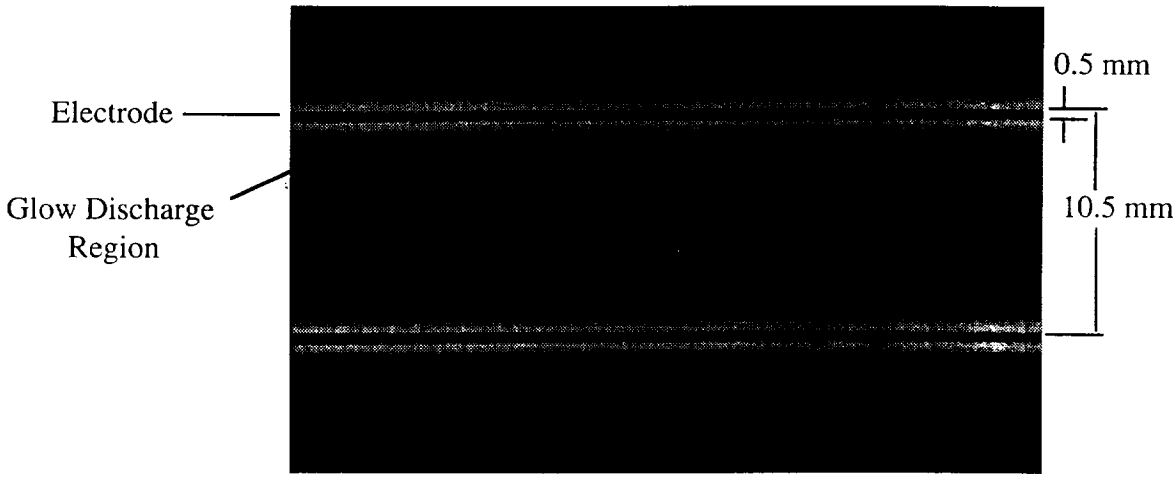

Figure 4. Portion of Model C7-C with plasma. E=3 kVrms, F=3 kHz. (Original photograph taken with 35mm 400 ISO color print film, approximately 10 second exposure.)

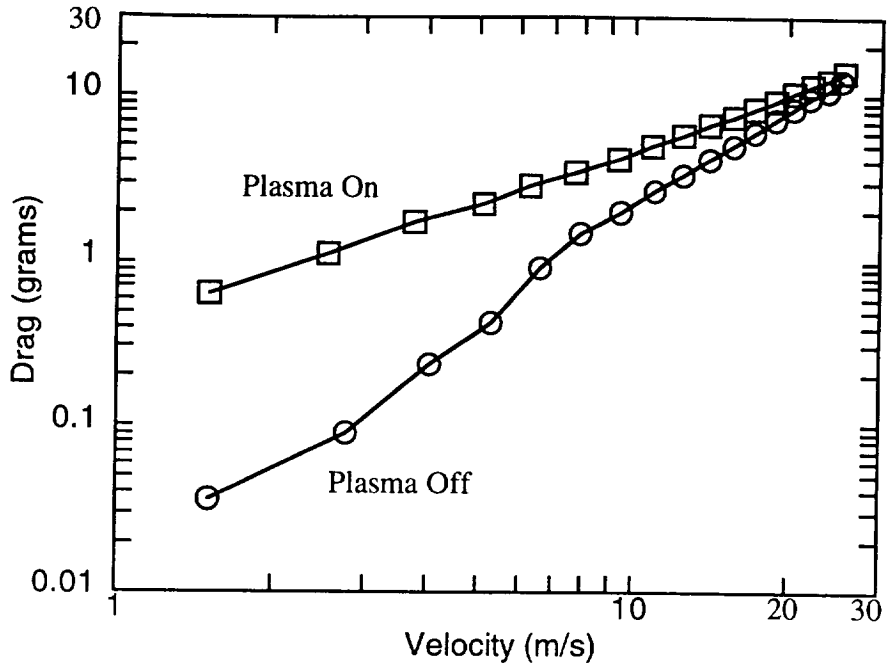

Figure 5a. Directly measured drag of panel C7-A (streamwise oriented electrodes) operated at 3.0 kHz and approx. 4.0 kV rms.

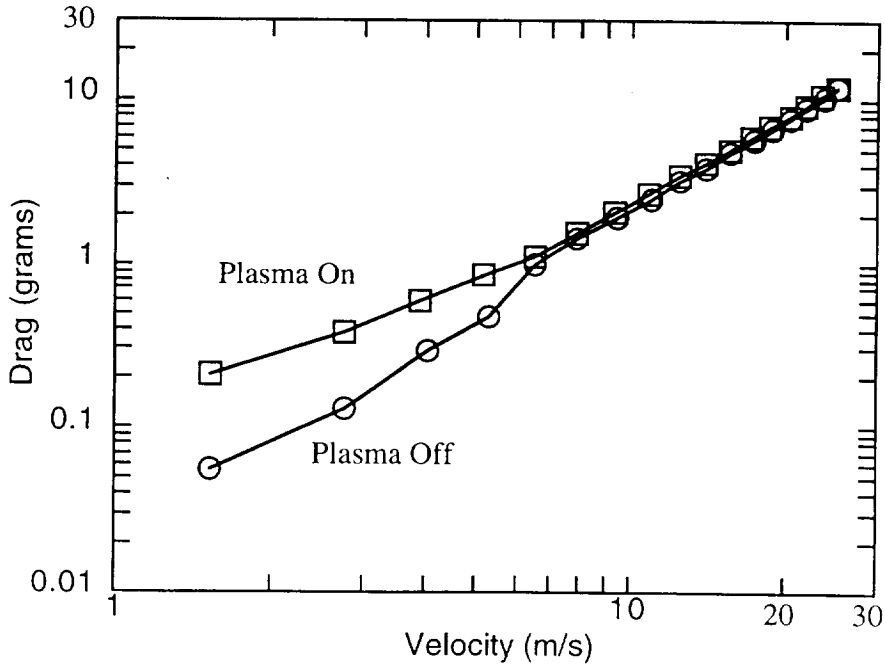

Figure 5b. Directly measured drag of panel C7-C (spanwise oriented electrodes) operated at 3.0 kHz and approx. 4.0 kV rms.

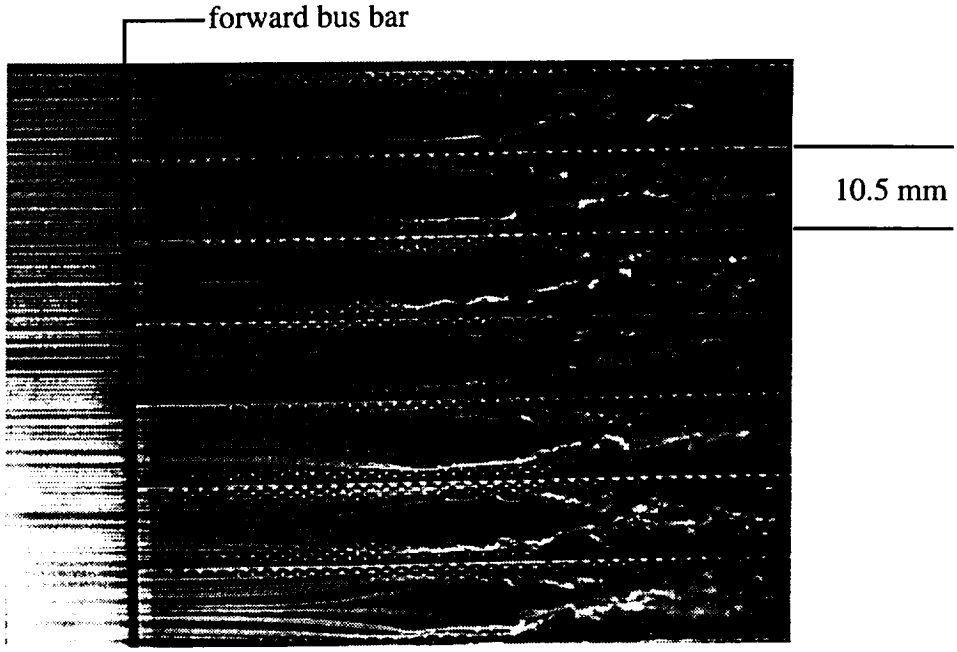

(a) E=3 kV rms, F=3 kHz

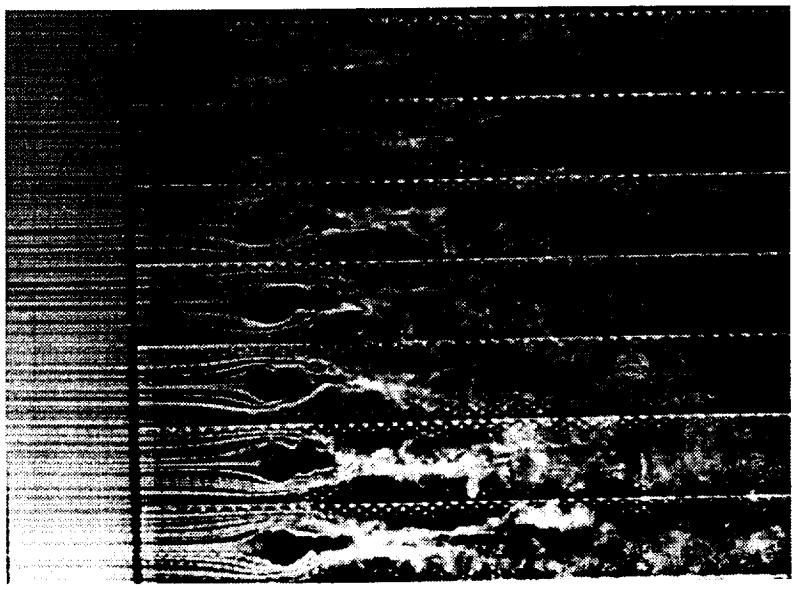

(b) E=5 kV rms, F=3 kHz

Figure 6(a,b,c). Smoke wire flow visualization of panel C7-A (streamwise upper electrodes with planar lower electrode) at two excitation voltages. $U_\infty = 4$ m/s. Smoke wire at Y=5 mm ($u/U_\infty \sim 0.65$). Images digitally enhanced with unsharp mask filter.

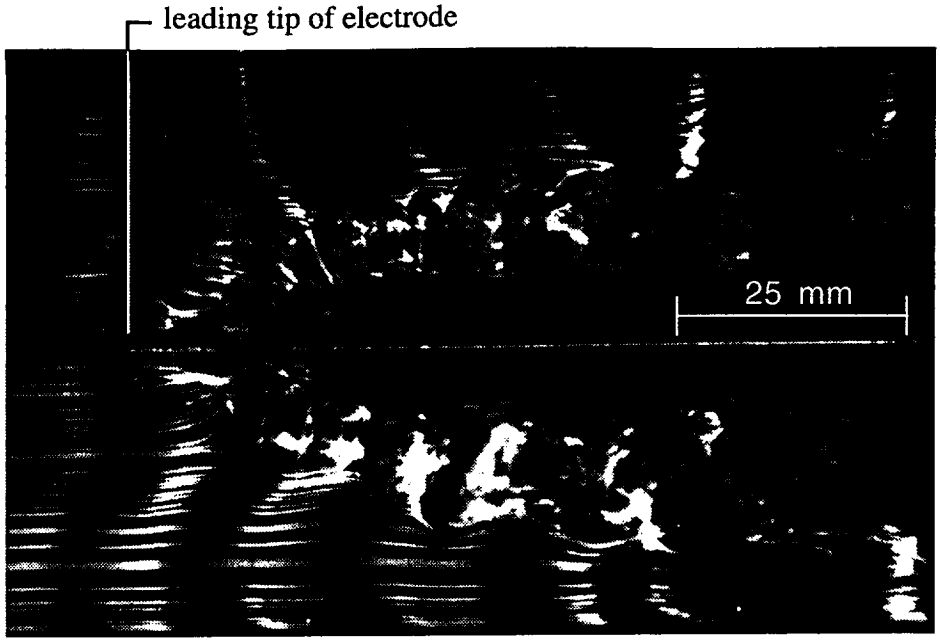

Figure 6(cont.) (c). Horizontal smoke wire flow visualization of a single electrode with symmetric plasma formation. The wire is at Y=2 mm. Stream velocity is 4 m/s.

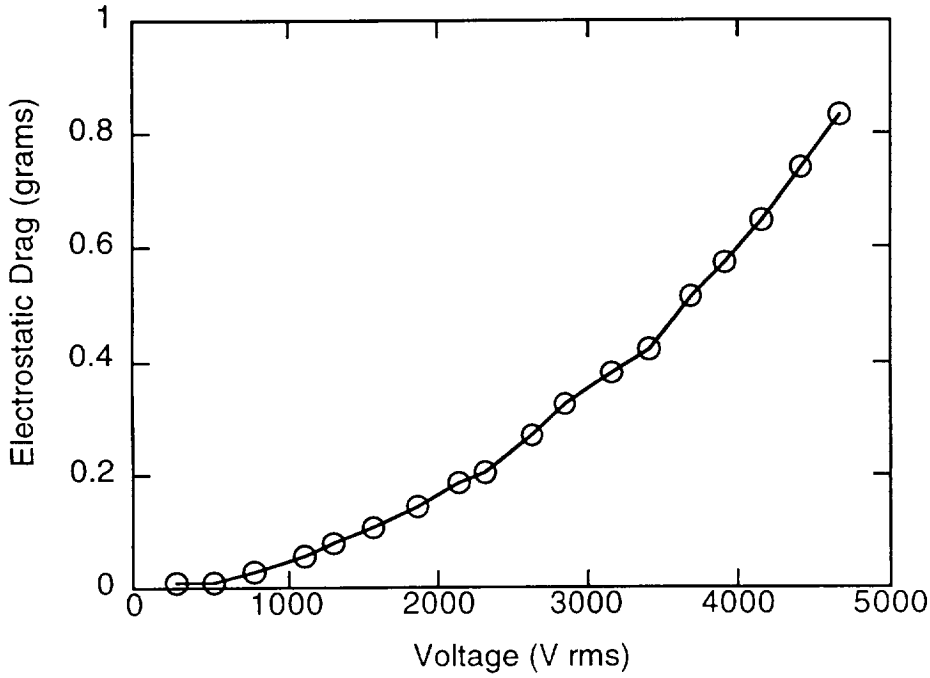

Figure 7. Electrostatic drag for panel C1-B (streamwise upper electrodes over planar lower electrode); F= 1.5 kHz, $U_\infty = 0$.

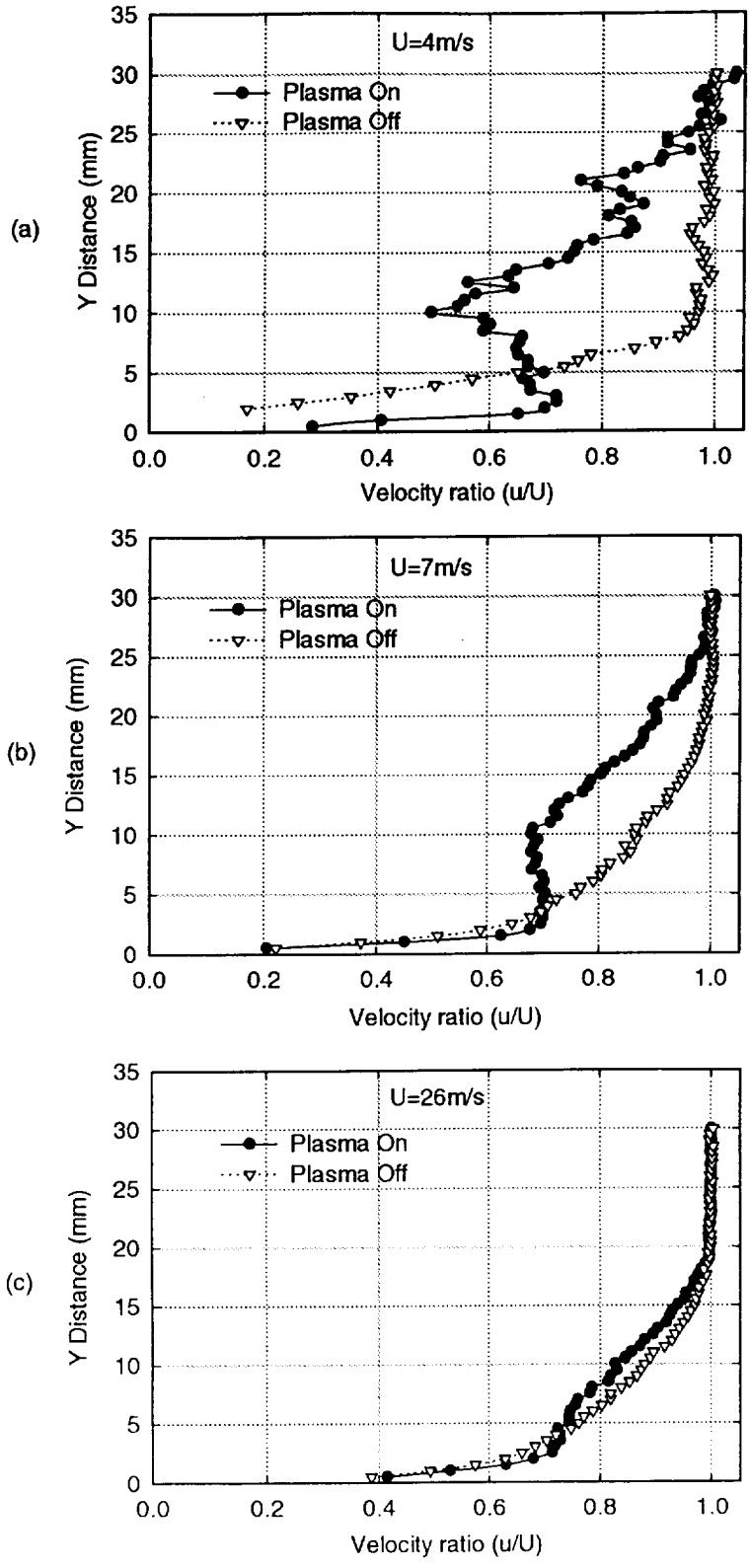

Figure 8 (a,b,c) Wall-normal velocity profiles for Panel C7-A (symmetric, streamwise electrodes; 3.0 kHz, 5.1 kV). Pitot tube located 28 mm downstream of the panel aligned between two adjacent electrodes.

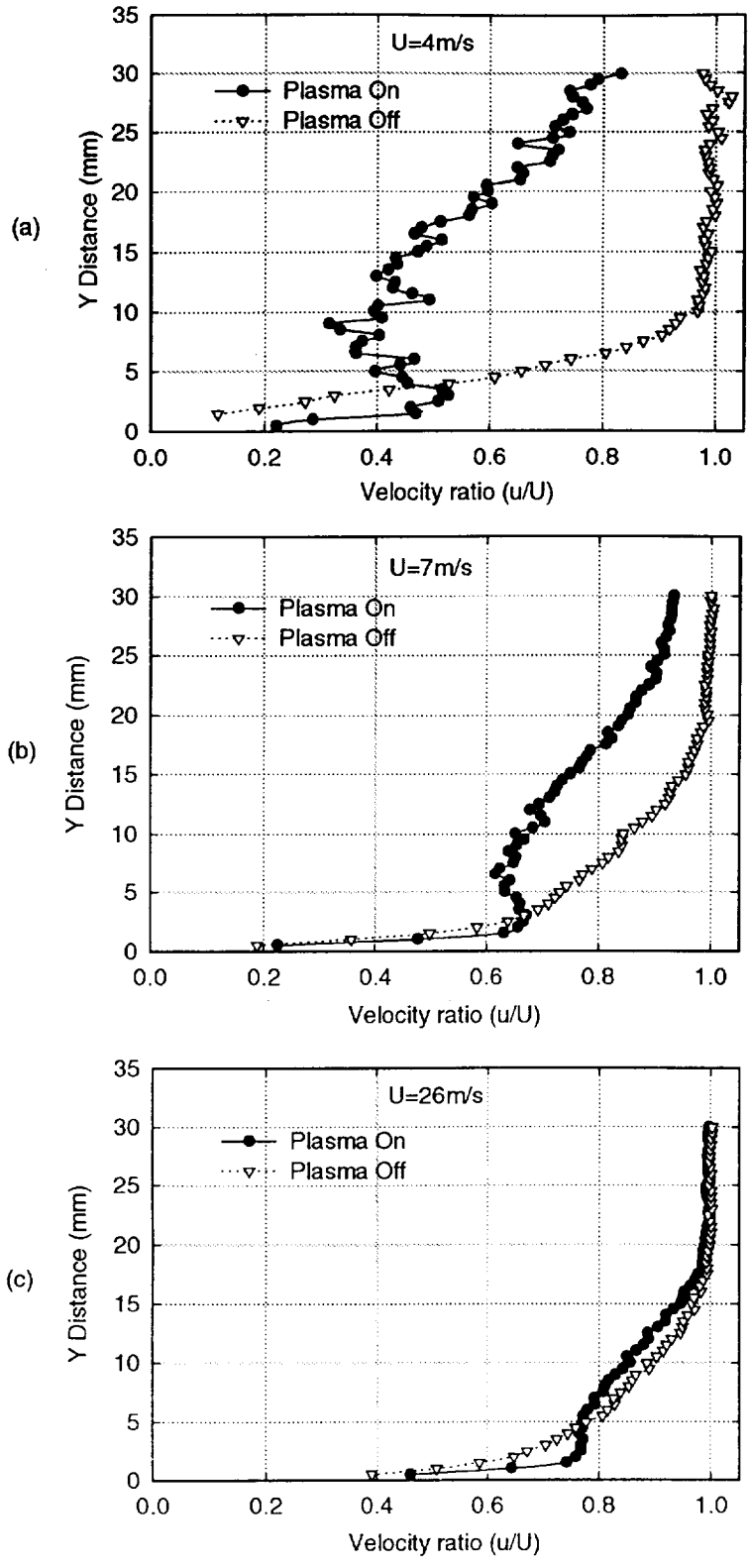

Figure 9 (a,b,c) Wall-normal velocity profiles for Panel C7-A (symmetric, streamwise electrodes; 3.0 kHz, 5.1 kV). Pitot tube located 28 mm downstream of the panel aligned directly behind an electrode.

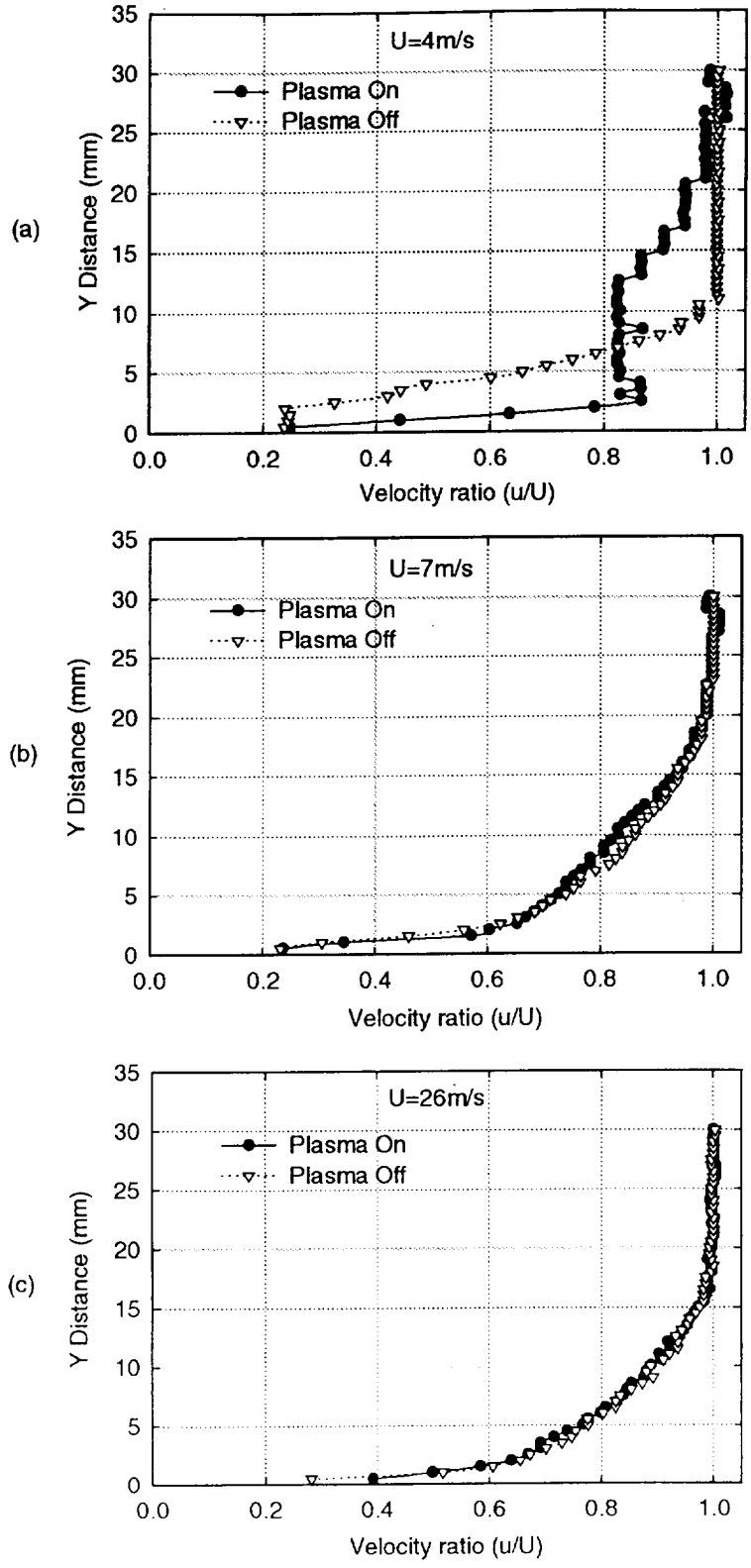

Figure 10a.,b.,c.) Pitot tube velocity profiles for Panel C7-C (with symmetric, span-wise electrodes; 3.0 kHz, 5.0 kV). Pitot tube located 28 mm downstream of last electrode.

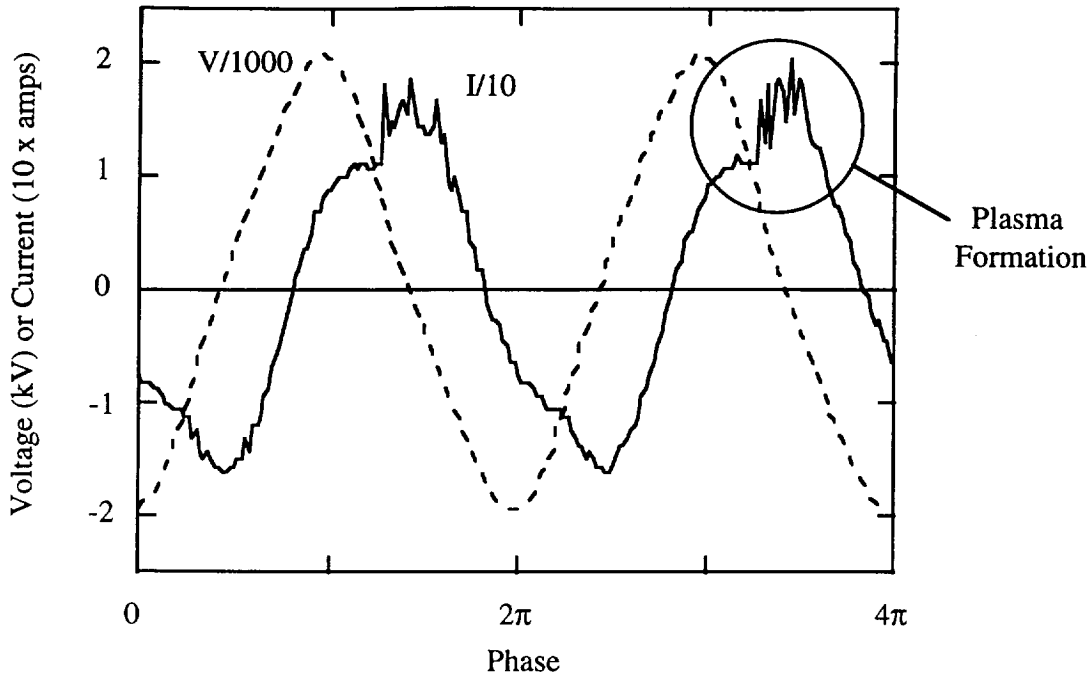

Figure 11. Example of instantaneous OAUGDP voltage and current waveforms. Showing plasma formation. Panel C1-C. Frequency 2.5 kHz.

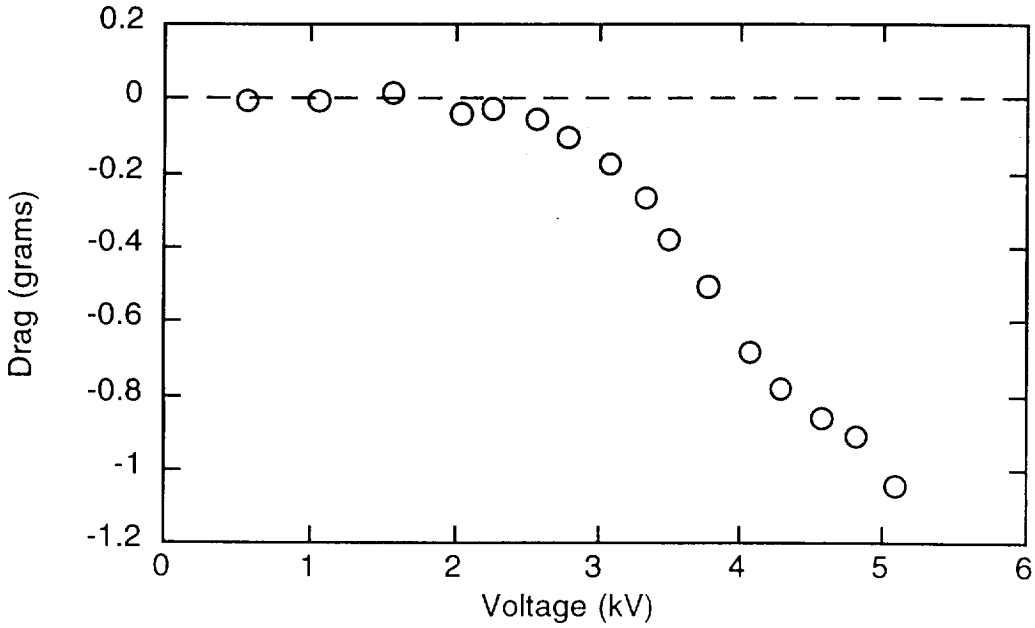

Figure 12. Electrostatic drag for panel E6-C in still air. Electrodes are spanwise, asymmetric with lower electrode staggered downstream relative to the upper electrode. Frequency: 3 kHz. Negative values correspond to a reduction in drag.

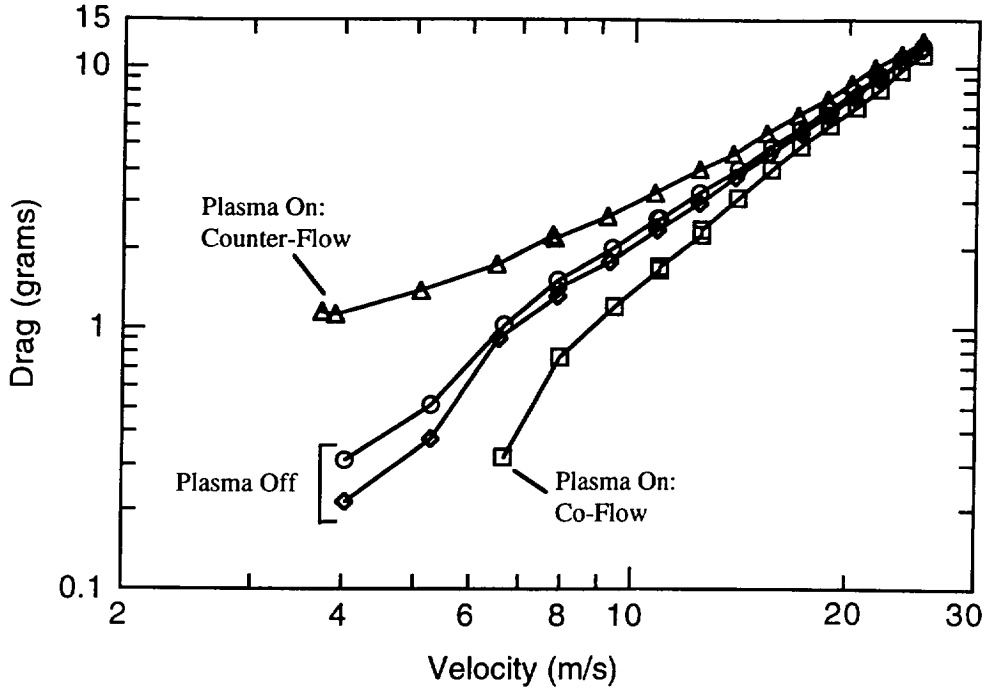

Figure 13. Directly measured drag of panel E6-C (spanwise, asymmetric electrodes, 3 kV, 4 kHz). Co-flow case corresponds to bottom electrode staggered downstream of top electrode; Counter-flow corresponds bottom electrode staggered upstream of top electrode.

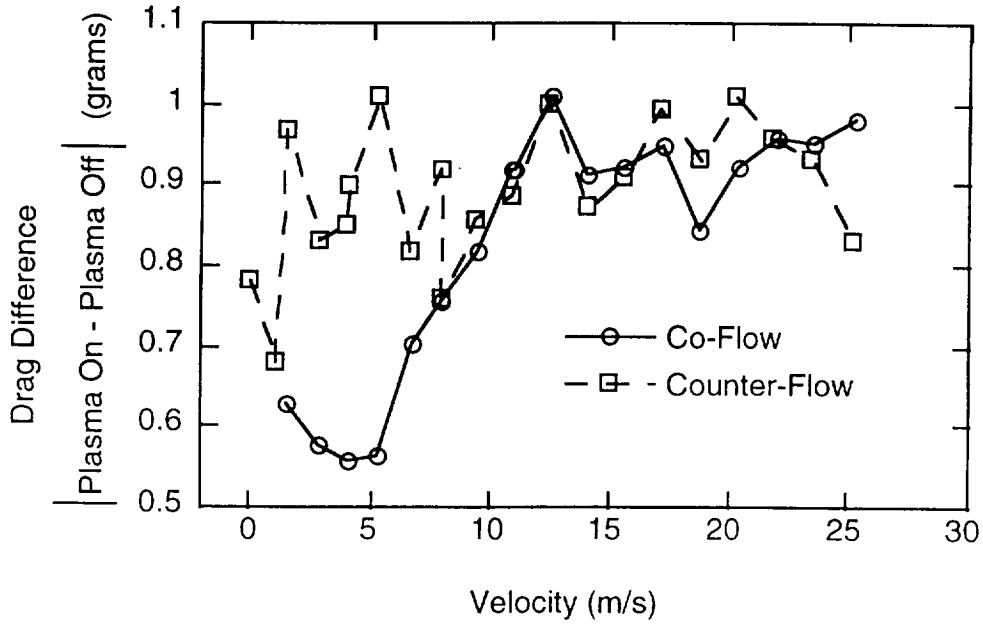

Figure 14. Drag change due to OAUGDP for panel E6-C in Co-flow and Counter-flow configurations (See Figure 13). Voltage and frequency were 4kV rms and 3kHz respectively.

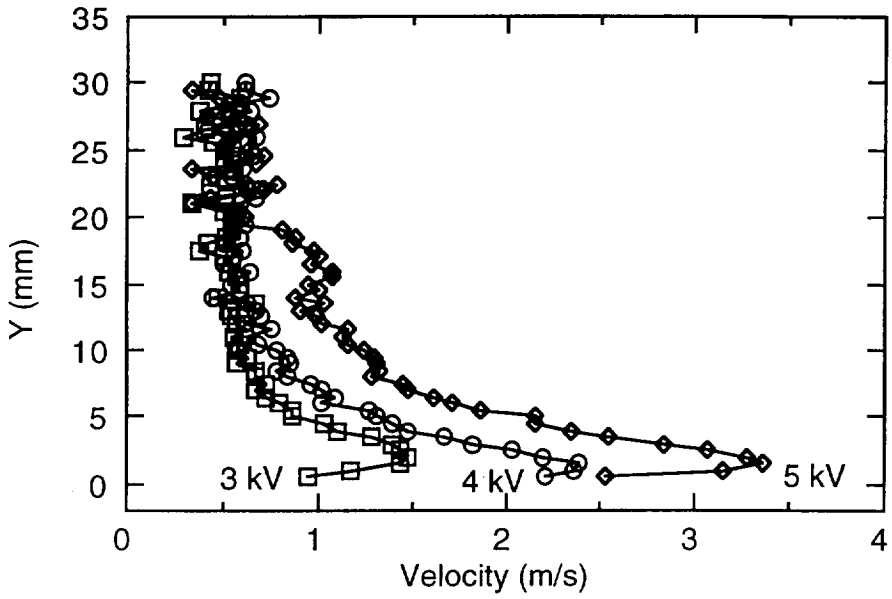

Figure 15. OAUGDP-induced velocity (blowing) along panel E6-C surface, normal to the electrodes. Frequency was 3 kHz. Measurements conducted in still air.

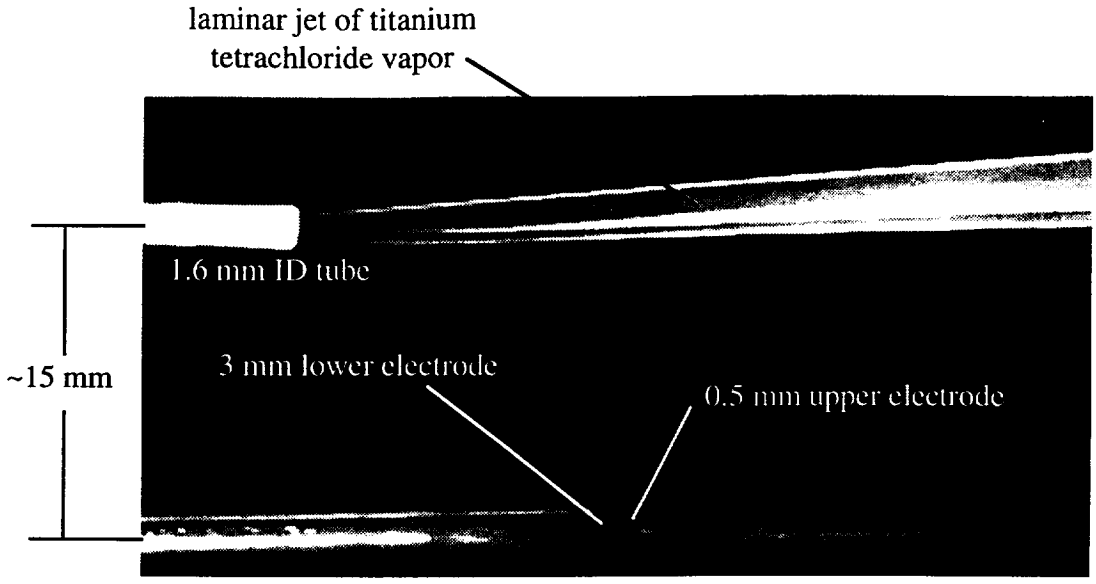

(a) Plasma Off

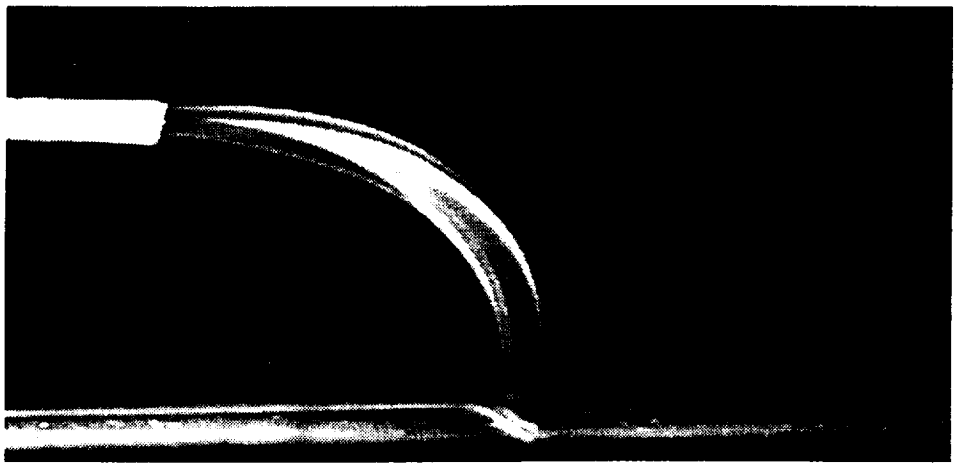

(b) Plasma On, E ~ 4.5 kV rms, F = 3 kHz

Figure 16(a,b). Demonstration of OAUGDP paraelectric force due to a single asymmetric electrode in still air. Model is a single 0.5 mm wide electrode on the upper surface with a 3 mm wide lower electrode offset to the left. Jet exit velocity is estimated be in the range of 1 to 2 m/s.